ACS Energy LETTERS

http://pubs.acs.org/journal/aelccp

Suppressing Shuttle Effect with a Size-Selective Covalent Organic Framework Based Bilayer Membrane

Alae Eddine Lakraychi, Erin S. Picton, Yanliang Liang, Devin L. Shaffer,* and Yan Yao*

Cite This: *ACS Energy Lett.* 2023, 8, 5032−5040

Read Online

ACCESS | Metrics & More | Article Recommendations | Supporting Information

ABSTRACT: **Organic batteries, while promising due to their abundant elements and minimal environmental impact, often suffer from capacity fade because of the shuttle effect of dissolved redox intermediates. To address this issue, we introduced a bilayer membrane, TpPa@PP, consisting of a 70-nm covalent organic framework (COF) thin film synthesized by interfacial condensation and subsequently deposited on a polypropylene substrate. This membrane allows solvent and ion transport, while rejecting soluble organic intermediates. When paired with pyrene-4,5,9,10-tetraone (PTO), an organic cathode with high capacity but notable dissolution issues, the TpPa@PP membrane effectively blocked the bulky PTO and Li_2-PTO species from crossover in an H-type cell, resulting in only a slight decrease in Li-ion flux. Furthermore, the membrane improved the first-cycle Coulombic efficiency. This work offers crucial insights into the membrane design for organic batteries.**

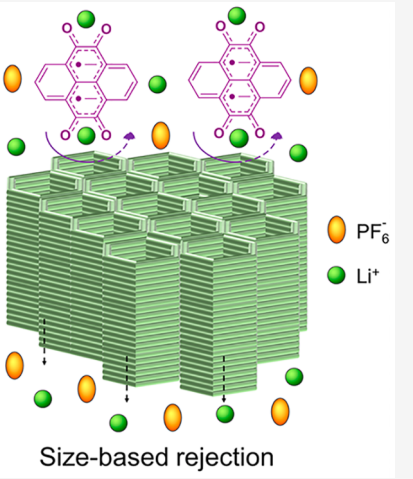

Over the past decade, tremendous efforts have been directed toward organic batteries, aiming to reduce the forthcoming market pressure on Li-ion batteries.[1] However, a major concern hampering the practical implementation of organic batteries is their rapid capacity decrease during electrochemical cycling. This issue stems from the loss of active material during the redox reaction in conventional electrolytes, involving one or more soluble redox intermediates.[2,3] Various approaches have been explored to address this persistent issue, including the modification of molecular structure by introducing ionic groups,[4−6] polymerization,[7−9] immobilization of organic species inside mesoporous carbon hosts,[10,11] and design of improved liquid[12] and solid-state electrolytes.[13] While these approaches have shown some success in alleviating the dissolution of redox intermediates in organic batteries, most have not completely suppressed it.

It is essential to recognize that mitigating dissolution often comes at a cost of cell-level specific energy due to factors such as increased molecular weight (via molecular modification), low impregnation rate (in carbon hosts), flooded high-concentration liquid electrolyte, or low active fraction (in solid-state electrolytes). As a result, there is an urgent need for a more efficient strategy to suppress dissolutionin organic batteries and achieve long-lasting stability without compromising cell-level specific energy.

Separator design has been overlooked in organic battery research, as it is often perceived as an inactive battery component. There are several compelling reasons to consider modified separators as a critical component of the battery design. First, the separator is the lightest component, in terms of both weight and cost. Second, with finely tuned pore sizes, the separator can play a crucial role in inhibiting targeted soluble active species from diffusional crossover while still allowing ion diffusion. This selective control of species transport contributes to enhanced battery cycling stability. Third, when properly designed, the separator can function as a secondary current collector, actively promoting the electrochemical conversion of redox organic species.[14]

Received: August 20, 2023
Revised: October 24, 2023
Accepted: October 30, 2023

https://doi.org/10.1021/acsenergylett.3c01740
ACS Energy Lett. 2023, 8, 5032−5040

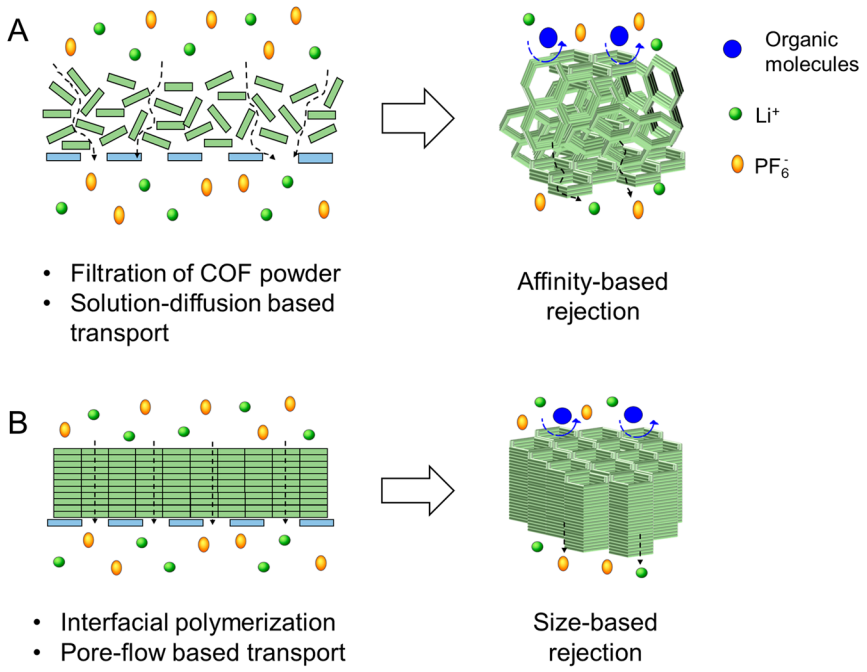

Figure 1. Schematic comparison of two methods for preparing bilayer COF membranes. (A) Conventional approach using filtration of COF powders and (B) our approach based on interfacial polymerization.

Functional separators have already found successful applications in Li-sulfur batteries, demonstrating encouraging results in suppressing the shuttle effect of soluble polysulfides.[15] In organic batteries, this separator modification strategy has recently emerged with a handful of studies showcasing its potential with organic molecules. For instance, Song et al. reported the use of a sandwich-type separator based on polypropylene/Nafion/polypropylene to effectively prevent the shuttle effect of an anthraquinone derivative.[16] Similarly, Li et al. demonstrated excellent cycling stability of another soluble anthraquinone derivative by using a gel polymer electrolyte (GPE) that forms *in situ* on a Nafion-coated separator.[17] Additionally, Bai et al. demonstrated the efficiency of a metal−organic framework (MOF) gel membrane separator in mitigating the shuttle of benzoquinone derivatives, leading to high cycling stabilities.[3]

Covalent organic frameworks (COFs) possess highly ordered structures, permanent porosity, a rigid network, and excellent chemical stability,[18] making them well-suited as battery separator materials which can significantly enhance cycling stability. Their ability to form molecularly thin membranes with a high density of aligned single-digit nanopores (SDNs) facilitates mass transport.[19] Moreover, the extensive knowledge about COF-based separation membranes in liquid-phase filtration can be extended to the battery field, enabling the exploration of other parameters such as electrochemical stability and chemical interactions with redox-active species and electrolyte.

COF-based bilayer membranes have shown promise in preventing the crossover of dissolved polysulfides in sulfur batteries, as reported by various research groups.[20−23] However, the understanding of solute rejection by the COF layer has not kept pace with experimental advancements. This is partly due to the limitations of conventional fabrication methods like filtration or coating, which result in bilayer membranes with large thickness (>1 μm) and random crystallite orientation in the COF layer (Figure 1 and Table S1). Mass transport in these bilayer membranes primarily occurs through interparticle pores, e.g., discontinuities and grain boundaries. This follows a transport model known as solution-diffusion,[24] and the molecules are rejected based on their affinity to the COF layer rather than by molecular size (Figure 1A). Ideally, bilayer membranes should be fabricated with well-oriented crystallites and uniform pores that extend through the membrane thickness. Consequently, mass transport in this case occurs through uniform and intrinsic permanent pores according to the pore-flow transport model,[24] where molecules are sieved strictly based on their molecular size relative to the pore size of the COF (Figure 1B). To achieve this goal, interfacial polymerization synthesis can be used, offering control over crystallite orientation in a large area.

In this work, we designed and fabricated a large-area bilayer membrane consisting of a thin enamine-based COF supported by a conventional polypropylene (PP) separator substrate. The COF was synthesized by interfacial condensation between 1,3,5-triformylphloroglucinol (Tp) and *p*-phenylenediamine (Pa) at a water−toluene interface. The resulting bilayer membrane, named TpPa@PP, effectively prevented bulky organic intermediates from diffusing across the membrane in an H-type cell, with only a slight reduction in Li-ion flux. Furthermore, in a Li-organic cell, the bilayer membrane significantly improved the first-cycle Coulombic efficiency and moderately increased the cycling stability. Lastly, our findings highlight crucial factors to consider when designing efficient membranes for organic batteries.

Pyrene-4,5,9,10-tetraone (PTO) was selected as the model organic active material for this study due to its excellent electrochemical properties in various battery chemistries, including acid batteries,[25] magnesium batteries,[2] and solid-

https://doi.org/10.1021/acsenergylett.3c01740
ACS Energy Lett. 2023, 8, 5032−5040

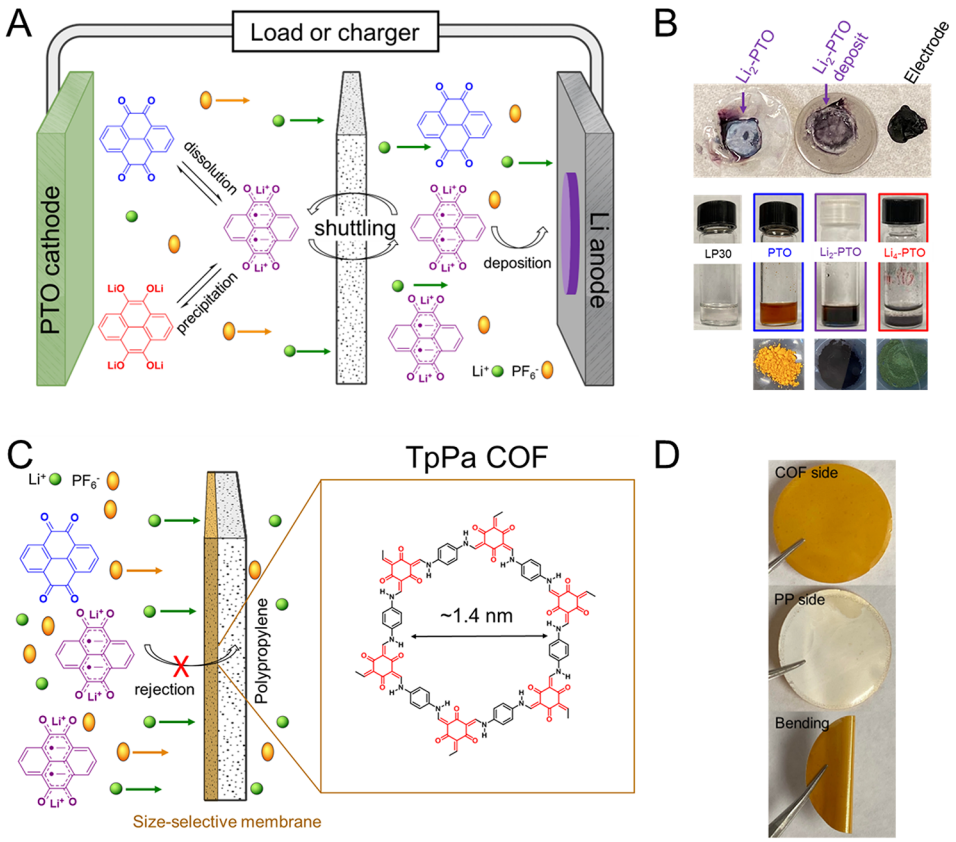

Figure 2. (A) Schematic diagram of the dissolution−precipitation reaction pathway in a PTO/Li cell highlighting the "shuttle effect" of Li_2-PTO to the anode through a porous separator. (B) Digital photographs of a dismantled PTO/PP/Li cell after cycling: (left) a PP separator covered with purple Li_2-PTO; (middle) Li metal surface with Li_2-PTO deposit; (right) the organic cathode after cycling. Solubility tests of PTO redox intermediates (10 mg of powder in 500 μL of LP30 electrolyte) and the corresponding powders of PTO, Li_2-PTO, and Li_4-PTO. (C) Schematic of a TpPa@PP bilayer membrane where the TpPa layer acts as a physical barrier toward blocking soluble Li_2-PTO. (D) Digital photographs of a TpPa@PP bilayer membrane.

state batteries,[26] and the fact that it has been well studied by our group. In a PTO/Li half-cell utilizing an organic liquid electrolyte, the PTO system follows a redox reaction pathway similar to that of sulfur[27] but with less complexity, resulting in a single intermediate, "PTO^{2-}", as shown in Figure 2A. During the discharge, the PTO molecule is first reduced to Li_2-PTO, which dissolves in the electrolyte due to its solubility and then continues to be reduced to precipitate the insoluble Li_4-PTO. The reverse process takes place during the charge. Unfortunately, this heterogeneous liquid−solid reaction path has a negative impact on the cycling stability of the PTO system because the soluble intermediate species could shuttle through the separator, corroding the surface of the Li metal and leading to a loss of active material.

To gain deeper insights into the PTO reaction pathway, we conducted the chemical synthesis of the intermediates and quantified the solubility of Li_2-PTO and Li_4-PTO, along with PTO, for the first time. Notably, we observed distinct color changes in the PTO powder depending on the degree of lithiation: yellow for PTO, purple for Li_2-PTO and green for Li_4-PTO (Figure 2B). In a carbonate-based electrolyte (LP30), Li_2-PTO was found to be the most soluble species, exhibiting a solubility of 0.12 mM (31.8 μg/mL), followed by PTO with a solubility of 0.08 mM (21 μg/mL), whereas Li_4-PTO was determined to be insoluble, likely due to its enhanced intramolecular interactions through O−Li−O bonding (Figure 2B and Figure S1). The images of the disassembled PTO/Li half-cell after cycling in Figure 2B provide further evidence of the solubility and migration of Li_2-PTO species during battery operation. The separator was visibly covered with a substantial amount of purple dissolved species (Li_2-PTO), which indicates severe dissolution. Simultaneously, the surface of the Li metal was also covered with the same species, suggesting the diffusion of Li_2-PTO and corrosion of the Li metal. The absence of yellow species (PTO) does not necessarily imply that PTO is not involved in this failure mechanism; rather, it could be masked by the intense purple color. These findings confirm that the Li-PTO system undergoes a heterogeneous liquid−solid redox reaction pathway and point toward the dissolution of both PTO and Li_2-PTO as the root cause for poor cycling stability.

To address the rapid capacity fade issue in organic batteries, we developed a bilayer membrane comprising a 70-nm-thick COF film (TpPa) on polypropylene substrate (PP), serving as a size-selective barrier to hinder the diffusion of soluble organic intermediate species (PTO and Li_2-PTO), as illustrated in Figure 2C. The TpPa COF film was synthesized using a modified Langmuir−Blodgett (LB) method at a water−toluene interface, following our previous report.[28] This resulted in a freestanding TpPa thin film that was then transferred onto a PP substrate placed at the bottom of the LB trough, thus fabricating the TpPa@PP bilayer membrane. We

https://doi.org/10.1021/acsenergylett.3c01740
ACS Energy Lett. 2023, 8, 5032−5040

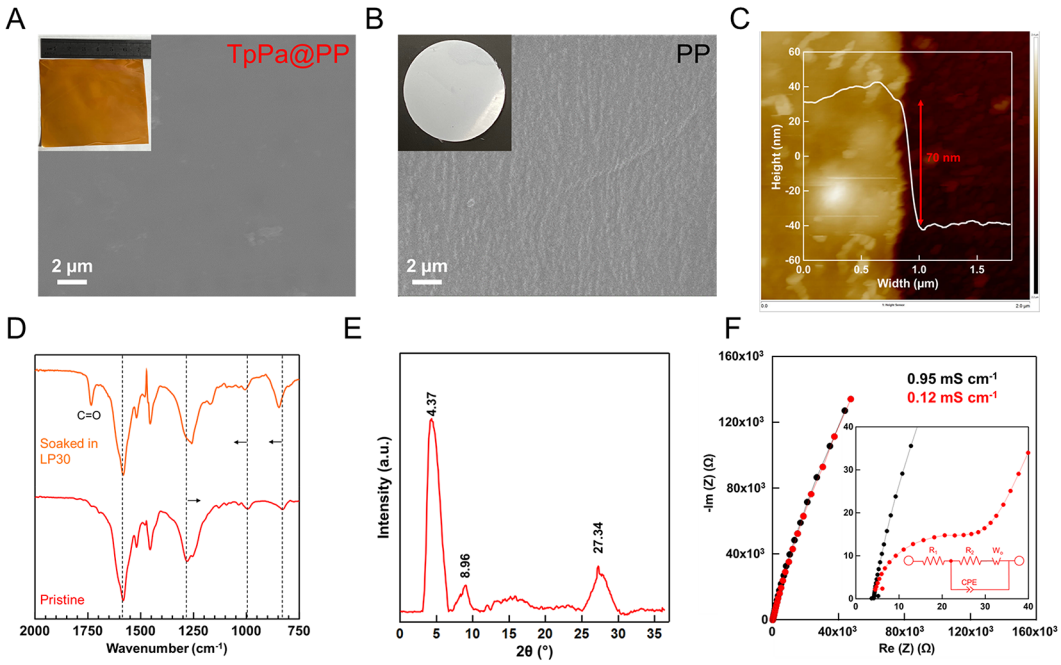

Figure 3. Characterizations of TpPa@PP bilayer membrane fabricated using the Langmuir−Blodgett method. (A, B) Top view SEM images for TpPa@PP and PP, respectively. The inset of (A) shows a large area (50 cm^2) of TpPa@PE membrane. (C) AFM height image and corresponding height profile of TpPa COF film on a Si/SiO_2 wafer. (D) FTIR spectra in the fingerprint region of pristine TpPa@PP and after soaking in LP30. The sample was washed with DMC and dried under vacuum at 60 °C overnight. The signal of a blank PP support was subtracted during the background measurement. (E) EWAXS (wavelength, λ = 0.154 nm) pattern of TpPa-COF film fabricated using the confined interface method (2θ refers to the scattering angle). (F) Ionic conductivities of LP30 electrolyte in the presence of TpPa@PP and PP separators determined by an AC impedance technique using a Swagelok cell. The inset shows a zoomed-in plot and an equivalent circuit.

successfully obtained a large-area (50 cm^2) membrane with no signs of delamination after being cut into smaller pieces, and its physical integrity remained unchanged even under bending stresses, as shown in Figure 2D.

Scanning electron microscopy (SEM) images of the TpPa@PP bilayer membrane in Figure 3A,B reveal a continuous, smooth, and defect-free TpPa layer uniformly covering the macroporous PP substrate. By conducting atomic force microscopy (AFM) on the TpPa film deposited on a silicon wafer (Figure 3C), we determined an average thickness of 70 ± 3 nm, which is much thinner than the PP thickness (25 μm). The TpPa film thickness can be readily adjusted by varying the monomer concentrations, providing flexibility in tuning the membrane's properties.[29] The Fourier transform infrared (FTIR) spectrum of the TpPa-COF film in the bilayer membrane (Figure 3D) closely matches the spectrum of TpPa-COF powder synthesized by mechanosynthesis (Figure S2).[30] The characteristic stretching bands at ~1574 (−C═C) and ~1256 cm^{-1} (−C−N) confirm the formation of a keto-enamine linkage, typical of the Schiff-base reaction. Notably, the absence of stretching bands at ~1645 ($-NH_2$) and ~1640 cm^{-1} (−C═O) indicates the absence of impurities from amine (Pa) or aldehyde (Tp) monomers, respectively, in the COF film (Figure S2). The diffraction pattern derived from extended wide angle X-ray scattering (EWAXS) measurements of our interfacially polymerized TpPa-COF is consistent with previously reported PXRD of the same COF synthesized by a solvothermal method,[31] indicating that the TpPa-COF layer used in our bilayer membrane is crystalline (Figure 3E). The intense peak at 2θ = 4.4° corresponds to the COF membrane pore size, reflected from the (100) plane, whereas the peak at 2θ = 27° is correlated to the $\pi-\pi$ stacking distance between the COF nanosheets that comprise the film. The minor peak revealed at $2\theta \approx 9°$ should correspond to the reflection plane (200).[31] Overall, the experimentally obtained pattern correlates very well with the simulated results for eclipsed stacking, rather than staggered stacking, indicating a hexagonal pore structure with a pore diameter of ~1.8 nm, in agreement with the report by Kandambeth et al.[31]

To explore the wettability of the electrolyte (LP30) on the TpPa@PP surface, we measured the contact angles, which showed a slightly lower contact angle of 40.9° compared with that of PP (45.1°), as shown in Figure S3. The reduced contact angle can be attributed to the intrinsic affinity between the COF and the polar solvent molecules in the electrolyte. This is further supported by the presence of the stretching band at 1739 cm^{-1} (−C═O) in the FTIR spectrum of the membrane after soaking it in the electrolyte (Figure 3D). This carbonyl band corresponds to the ester group in the dimethyl carbonate (DMC) molecules present in the electrolyte. The presence of DMC as a structural component (not residual) is evident, as some characteristic bands were shifted, while the most intense band at ~1574 cm^{-1} remained unchanged. These findings suggest the existence of plausible solid−liquid interactions at the nanoscale, which may influence mass transport in SDNs. The TpPa@PP membrane, owing to its chemically robust and highly stable keto-enamine linkage, exhibits excellent chemical stability in the electrolyte solution and maintained its morphology and chemical structure after immersion in the electrolyte for over 1 month.

Figure 3F shows the AC impedance spectra of TpPa@PP and bare PP. Both cells exhibit inclined lines with bulk resistances of 4.29 and 4.13 Ω for the bilayer membrane and PP, respectively. Notably, TpPa@PP exhibits an additional

https://doi.org/10.1021/acsenergylett.3c01740
ACS Energy Lett. 2023, 8, 5032−5040

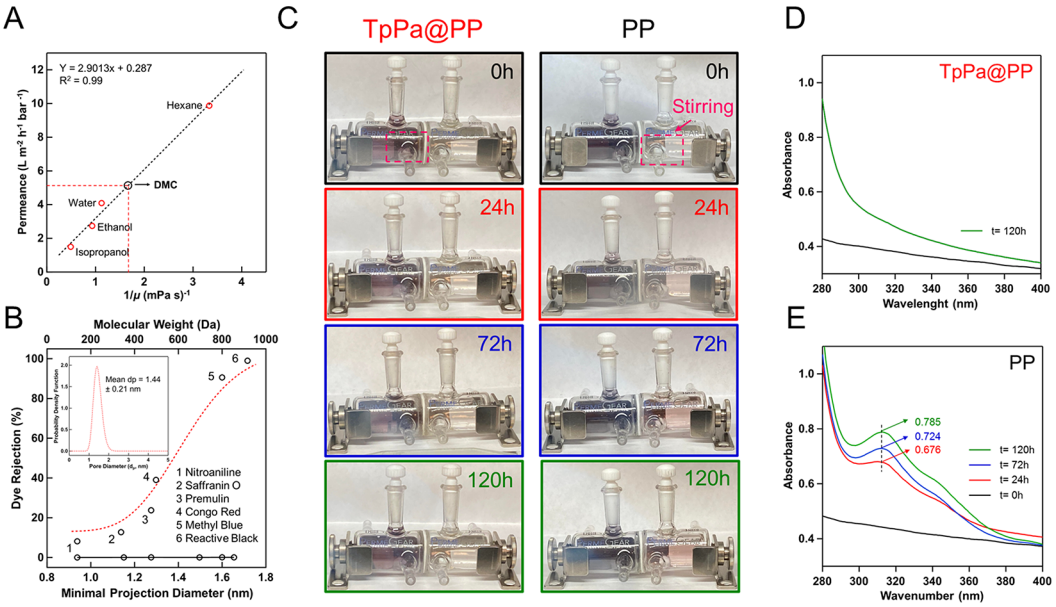

Figure 4. Solvent permeance and Li_2-PTO rejection test of a TpPa@PP bilayer membrane. (A) Permeances of various polar and nonpolar solvents for TpPa@PP plotted as a function of inverse solvent viscosities. The permeance of DMC was estimated from its viscosity at 25 °C (0.585 mPa s). (B) Rejection of solutes from ethanol solutions plotted as a function of molecular weight for MWCO determination and as a function of solute diameter for TpPa@PP and PP. The inset shows the calculated pore size distribution from log-normal cumulative distribution function fitting of the rejection curve. Solvent permeance occurs through permanent TpPa@PP membrane pores via pore-flow mass transport, and solute rejection occurs through size-based sieving. (C) Diffusion of Li_2-PTO species in an H-type cell through TpPa@PP and PP, respectively. (D, E) Corresponding UV−visible absorption spectra measured after different interval times.

depressed semicircle in the high-frequency impedance, corresponding to a charge transfer resistance of 32.48 Ω. This resistance could arise from various factors, such as Li^+ migration within the COF layer, a strong solvent−COF interaction, or desolvation of Li^+ when the solvation shells in LP30 electrolyte are larger than the pore size of the COF.[32,33] Distinguishing the dominant factor and elucidating the transport mechanism are complex and will be reported in our future work. The calculated ionic conductivity of using TpPa@PP and bare PP are 0.12 and 0.95 mS cm^{-1}, respectively. This difference in ionic conductivity could be associated with the aforementioned reasons and could potentially be enhanced by incorporating functional groups such as $-SO_3^-$ and oligo(ethylene oxide)[34] side chains within the pores to facilitate the coordination and dissociation of Li ions, offering a pathway for improving ion transport.

The TpPa@PP membranes were further evaluated by measuring solvent permeance and solute rejection. Dead-end filtration experiments were conducted using various solvents, and dye rejection was measured for dyes with different molecular weights and dimensions (ranging from 140 to 990 Da and between 9 and 17 Å in Table S2). Figure 4A shows that solvent permeance through the TpPa@PP membrane was inversely linearly related to solvent viscosity, indicating Hagen−Poiseuille pore flow,[35,36] thus supporting the eclipsed hexagonal pore structure of the COF layer. At a relatively high thickness to pore size aspect ratio of 50, pore entry effects are not expected to significantly contribute to mass transport.[37,38] Based on the established pore flow relationship, the permeance of the DMC electrolyte used in the half-cell studies is estimated to be ~5 L m^{-2} h^{-1} bar^{-1}.

The TpPa@PP membrane exhibited a molecular weight cutoff (MWCO) of ~800 Da, corresponding to 90% rejection of the methyl blue dye, as shown in Figure 4B. A MWCO could not be established for the bare PP, as it demonstrated low solute rejection for all dyes due to its relatively large pore size. To estimate the pore size distribution of the TpPa@PP membrane, a log-normal cumulative distribution function was fitted to dye rejection data expressed as a function of dye minimal projection diameter. The corresponding probability density function is shown in the inset to Figure 4B. The average pore diameter of the TpPa@PP separator was estimated to be 1.44 ± 0.21 nm, slightly smaller than that estimated from PXRD data and previously reported values for TpPa COF.[30] This difference in pore size may be attributed to increased pore tortuosity resulting from amorphous regions in the COF film or staggered rather than fully eclipsed stacking of individual COF nanosheets. Therefore, based on these results, we establish that solvent permeance occurs through permanent TpPa@PP membrane pores via pore-flow mass transport, and solute rejection occurs through size-based sieving.

To assess the effectiveness of the TpPa@PP membrane in suppressing the shuttle effect, we conducted rejection experiments with Li_2-PTO in an H-type cell filled with LP30 electrolyte. In the left chamber, we introduced the electrolyte containing Li_2-PTO, while the right chamber was filled with the blank electrolyte. The TpPa@PP membrane served as the separator between the chambers, and we maintained continuous stirring near the membrane surface to minimize concentration polarization. Over a prolonged period of 120 h, the dissolved Li_2-PTO species were unable to diffuse through the membrane, as was evident from the colorless appearance of the blank electrolyte in the right chamber (Figure 4C). Similar experiments were conducted with PTO, and they also showed the inability of PTO species to diffuse over the same period of 120 h (Figure S4). These findings demonstrate that the TpPa COF layer effectively blocked the diffusion of both Li_2-PTO and the PTO species.

https://doi.org/10.1021/acsenergylett.3c01740
ACS Energy Lett. 2023, 8, 5032−5040

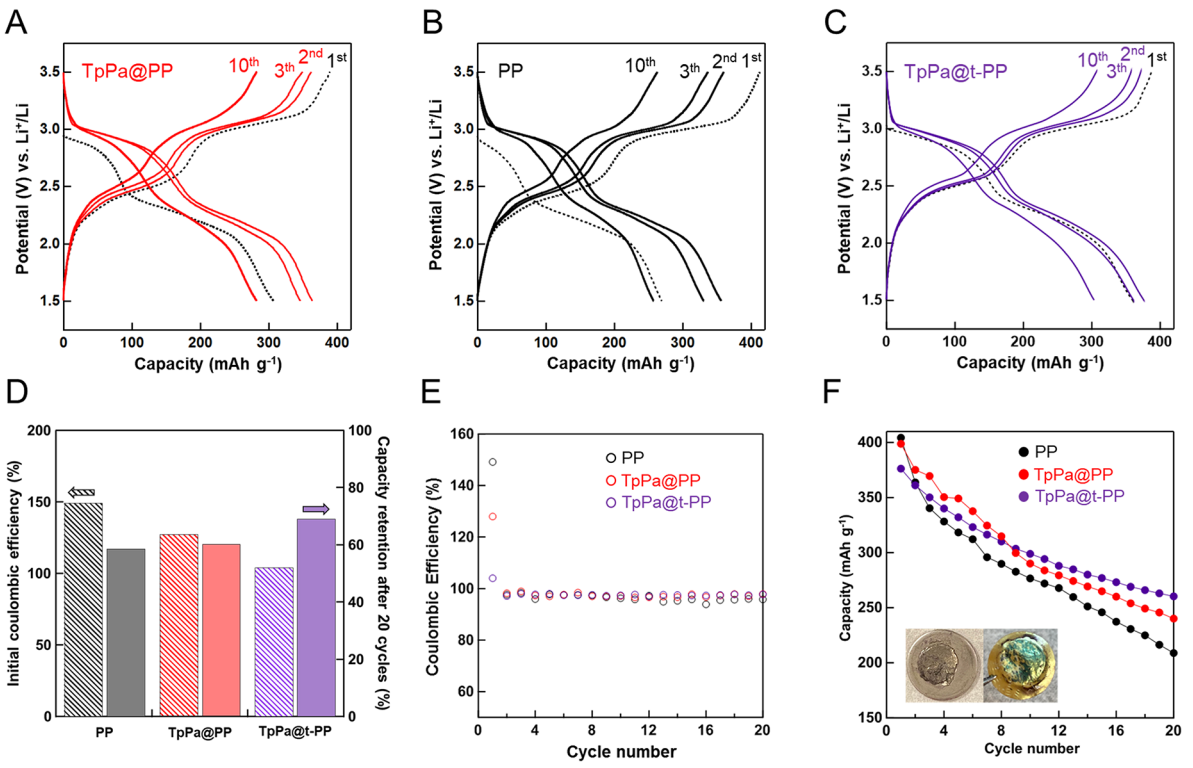

Figure 5. Electrochemical measurements of PTO/Li cells using different membranes. (A–C) Galvanostatic cycling voltage profiles for PTO/Li cells using TpPa@PP (A), PP (B), and TpPa@t-PP (C). t-PP stands for O_3/UV-treated PP. (D) Initial Coulombic efficiency and capacity retention comparison after 20 cycles using different membranes. (E) Comparison of Coulombic efficiency stability over 20 cycles. (F) Capacity retention over 20 cycles. The inset shows photographs of a clean Li metal surface and green powder on the cathode side of the TpPa@t-PP membrane after 20 cycles.

In contrast, when bare Celgard was used as the separator, the Li_2-PTO species easily permeated through it, driven by the concentration gradient across the separator. Within 24 h, the blank electrolyte in the right chamber became colored, and the intensity of the color increased after 120 h. We periodically analyzed the blank electrolyte in the right chamber by ultraviolet–visible spectroscopy. For TpPa@Celgard, the absorption spectrum of the blank electrolyte remained unchanged over an extended period of time, as shown in Figure 4D. However, for the initial blank electrolyte with the bare Celgard separator, we observed the increasing presence of a broad peak at ~312 nm, corresponding to the absorption band of Li_2-PTO. This indicates a continuous increase in the concentration of Li_2-PTO species in the right chamber, which is characteristic of continuous crossover.

These rejection experiments demonstrate the remarkable ability of the TpPa@Celgard membrane to effectively block the diffusion of soluble organic species such as Li_2-PTO and PTO. The bilayer membrane was then tested in a PTO/Li half-cell, as shown in Figure 5. As is typical with PTO-based liquid cells, the galvanostatic charge–discharge profile displays two distinct plateaus at around 2.90 and 2.25 V vs Li^+/Li, resulting in specific capacities of 307 and 391 mAh g^{-1} during the first discharge and charge, respectively. This leads to an initial Coulombic efficiency (ICE) of 127% when TpPa@Celgard is used as the separator (Figure 5A,D). In contrast, the reference cell with Celgard (Figure 5B,D) showed similar electrochemical behavior but with a much lower initial discharge capacity of 269 mAh g^{-1} and a slightly higher charge capacity of 403 mAh g^{-1}, resulting in a higher ICE reaching 149%.

Interestingly, during the initial discharge, both cells deliver less than 100 mAh g^{-1} for the upper plateau, which is much less than the expected capacity for the two electrons exchanged during the reaction from PTO to Li_2-PTO; whereas 200 mAh g^{-1} is achieved for the lower plateau, which accurately corresponds to the two electrons exchanged during the transition from Li_2-PTO to Li_4-PTO. Upon charging, the total capacity for four electrons is equally divided between the two plateaus. This behavior is characteristic of self-discharge in the cell, resulting from the dissolution of PTO particles in the cathode electrode during the 3 h rest time. In the case of PP, this phenomenon is exacerbated, probably due to the crossover of the PTO species.

Upon subsequent cycles, both cells exhibit capacity fading, although the cell using the TpPa@PP membrane showed slightly better retention (Figure 5A,B). For instance, the capacity retention at the 10th cycle is 72% for TpPa@PP and 63% for pristine, while the CE remains stable and close to 100% after the first cycle (Figure 5E). Notably, the membrane remains chemically stable within the studied electrochemical window upon cycling, thanks to the high stability of the imine-ketone (C=N) linkage (Figure S5). However, the membrane might be unstable at voltages <1.3 V vs Li^+/Li, where a Schiff base function is reported to be redox active.[39] Furthermore, the COF layer does not seem to react with PTO intermediate species, since mixing of both compounds does not lead to any apparent chemical reaction (Figure S5). Based on the excellent rejection properties observed in the H-type cell, the TpPa@PP cell was expected to show a significant improvement in cycling stability. However, the discrepancy in H-type cell and half-cell

https://doi.org/10.1021/acsenergylett.3c01740
ACS Energy Lett. 2023, 8, 5032–5040

performance can be attributed to the device configuration and testing conditions. In contrast to the H-type cell, the membrane in a coin cell is subjected to internal pressure, which could dislodge the TpPa layer if it is not securely adhered to the surface of the PP.

To address this issue, we treated the surface of PP with UV−ozone to enhance its adhesion with the TpPa layer,[40] and the resulting membrane is named TpPa@t-PP. Note that the TpPa layer was not exposed to this treatment. The TpPa@t-PP membrane demonstrated a significant improvement of the ICE (104.1%), and the capacity retention was further improved to 81% compared to 72% for TpPa@PP. This trend was maintained also after the 20th cycle, where the cell with TpPa@t-PP exhibits the highest capacity retention of 69%, whereas those with TpPa@PP and bare PP attain 60% and 59%, respectively.

The observed persistent capacity fade suggests that additional issues independent of crossover are present. To investigate this unexpected performance, the cell was disassembled after cycling and the membrane was examined (Figure S6). The SEM images show the presence of numerous irregularly shaped particles that were deposited from the PTO reaction during battery operation. Based on the green color of these particles, they are likely to be Li_4-PTO, which precipitated at the cathode-side membrane surface due to its insolubility. The precipitated Li_4-PTO particles are electrically isolated from the cathode and physically block the entrance of the ion into the membrane, which could explain the observed capacity decay. However, this observation supports the reduced crossover of PTO and Li_2-PTO species, as evidenced from the clean surface of the Li metal after cycling (inset of Figure 5F in contrast to Figure 2B). Adding two layers of carbon paper with a PTO electrode sandwiched in between slightly enhances the cycling stability from 72% to 77% after the 10th cycle (Figure S7). The benefit of carbon paper was more effective in the first cycle, where full utilization of the active material was achieved due to the reactivation of dissolved PTO species. However, the fouling issue was not fully solved, as can be seen by the apparent green deposits on the membrane after cycling (Figure S7). The origin of fouling might be attributed to various factors, such as lack of a conductive layer on the membrane to reactivate the deposited particles or intermolecular interaction between the COF layer and solute (Li_4-PTO). Understanding and solving this issue will be the subject of future work.

This work demonstrated that preventing the crossover of dissolved intermediates alone is insufficient to obtain high cycling stability, as additional issues such as fouling may occur and lead to capacity fade. An ideal bilayer membrane should be designed with respect to the redox organic intermediates, considering multiple factors such as suitable pore size and shape as a physical barrier to redox intermediates, chemical functionalization through electrostatic repulsion to modify the solvation microenvironment and ion transport through the membrane, an electronically conductive coating on the cathode side of the membrane to increase the utilization of precipitated redox organic species, and optimized membrane thickness to reduce the ionic transport resistance and increase ion flux. The optimal combination of these parameters could enable the development of organic batteries with excellent cycling stability.

Though interfacial polymerization is currently the preferred method to fabricate bilayer membranes with controllable thickness and crystallite orientation, it has its challenges, such as a long reaction time (3 days) and the need for a stable liquid−liquid interface. Therefore, synthesizing COF films with a shorter reaction time[41] directly on the supporting material, bypassing the liquid−liquid interface, would enhance scalablility for an industrially relevant roll-to-roll manufacturing process.

In conclusion, this work identifies the dissolution of the intermediate Li_2-PTO as the primary origin of the poor cyclability for the PTO/Li system. To tackle this, we developed a large-area 70-nm-thick TpPa COF film on commercial polypropylene separators using a modified Langmuir−Blodgett method. The interfacial polymerization synthesis afforded nanometer-scale precision in COF thickness while enabling tunablility of the support layer independently from the COF layer. We conducted a permeation study and small-molecule rejection test to determine the transport properties and pore size distribution of the TpPa@PP membrane, which exhibited pore-flow solvent transport with size-based solute rejection. Our results showed that TpPa@PP effectively blocked the crossover of Li_2-PTO with a minimal reduction in Li^+ ion transport. In the PTO/Li cell, TpPa@PP exhibited significantly improved first-cycle Coulombic efficiency and slightly enhanced cycling stability, which may have been limited by the fouling of Li_4-PTO species on the cathode side of the membrane. Finally, we proposed a COF-based membrane design to further improve the performance of organic batteries. By optimizing the bilayer membrane design and fabrication process, organic batteries could offer a promising alternative for energy storage with enhanced cycling stability, paving the way for their practical implementation.

■ ASSOCIATED CONTENT

Supporting Information

The Supporting Information is available free of charge. The Supporting Information is available free of charge at https://pubs.acs.org/doi/10.1021/acsenergylett.3c01740.

Detailed description of materials and fabrication of TpPa membrane and experimental methods, including PTO-based species solubility evaluation using UV−vis spectroscopy, FTIR spectroscopy, SEM, AFM, and contact angle measurements, EWAXS measurements, permeation experiments and characteristics of dye solutes, conductivity measurements, electrochemical performance testing, FTIR spectra for TpPa monomers, powder, and membranes before and after cycling, static contact angles of LP30 electrolyte on PP and TpPa membranes, H-cell diffusion experiments, photograph and SEM micrographs of TpPa membrane after cycling, and galvanostatic charge/discharge curves of PTO/Li cell (PDF)

■ AUTHOR INFORMATION

Corresponding Authors

Yan Yao − *Department of Electrical and Computer Engineering, University of Houston, Houston, Texas 77204, United States; Texas Center for Superconductivity at the University of Houston, Houston, Texas 77204, United States;* orcid.org/0000-0002-8785-5030; Email: yyao4@uh.edu

Devin L. Shaffer − *Department of Civil and Environmental Engineering, University of Houston, Houston, Texas 77204,*

https://doi.org/10.1021/acsenergylett.3c01740
ACS Energy Lett. 2023, 8, 5032−5040

United States; orcid.org/0000-0003-4583-1783; Email: dshaffer@uh.edu

Authors

Alae Eddine Lakraychi − *Department of Electrical and Computer Engineering, University of Houston, Houston, Texas 77204, United States; Texas Center for Superconductivity at the University of Houston, Houston, Texas 77204, United States*

Erin S. Picton − *Department of Civil and Environmental Engineering, University of Houston, Houston, Texas 77204, United States*

Yanliang Liang − *Department of Electrical and Computer Engineering, University of Houston, Houston, Texas 77204, United States; Texas Center for Superconductivity at the University of Houston, Houston, Texas 77204, United States;* orcid.org/0000-0001-6771-5172

Complete contact information is available at: https://pubs.acs.org/10.1021/acsenergylett.3c01740

Notes

The authors declare no competing financial interest.

■ ACKNOWLEDGMENTS

This work was supported by the University of Houston's National Centers Planning Award. E.S.P. acknowledges research support from the National Science Foundation (Award #2046453).

■ REFERENCES

(1) Poizot, P.; Gaubicher, J.; Renault, S.; Dubois, L.; Liang, Y.; Yao, Y. Opportunities and Challenges for Organic Electrodes in Electrochemical Energy Storage. *Chem. Rev.* **2020**, *120* (14), 6490−6557.

(2) Dong, H.; Tutusaus, O.; Liang, Y.; Zhang, Y.; Lebens-Higgins, Z.; Yang, W.; Mohtadi, R.; Yao, Y. High-power Mg batteries enabled by heterogeneous enolization redox chemistry and weakly coordinating electrolytes. *Nature Energy* **2020**, *5* (12), 1043−1050.

(3) Bai, S.; Kim, B.; Kim, C.; Tamwattana, O.; Park, H.; Kim, J.; Lee, D.; Kang, K. Permselective metal-organic framework gel membrane enables long-life cycling of rechargeable organic batteries. *Nat. Nanotechnol.* **2021**, *16* (1), 77−84.

(4) Renault, S.; Gottis, S.; Barrès, A.-L.; Courty, M.; Chauvet, O.; Dolhem, F.; Poizot, P. A green Li-organic battery working as a fuel cell in case of emergency. *Energy Environ. Sci.* **2013**, *6* (7), 2124−2133.

(5) Lakraychi, A. E.; Fahsi, K.; Aymard, L.; Poizot, P.; Dolhem, F.; Bonnet, J. P. Carboxylic and sulfonic N-substituted naphthalene diimide salts as highly stable non-polymeric organic electrodes for lithium batteries. *Electrochem. Commun.* **2017**, *76*, 47−50.

(6) Lakraychi, A. E.; Deunf, E.; Fahsi, K.; Jimenez, P.; Bonnet, J. P.; Djedaini-Pilard, F.; Bécuwe, M.; Poizot, P.; Dolhem, F. An air-stable lithiated cathode material based on a 1,4-benzenedisulfonate backbone for organic Li-ion batteries. *Journal of Materials Chemistry A* **2018**, *6* (39), 19182−19189.

(7) Nokami, T.; Matsuo, T.; Inatomi, Y.; Hojo, N.; Tsukagoshi, T.; Yoshizawa, H.; Shimizu, A.; Kuramoto, H.; Komae, K.; Tsuyama, H.; et al. Polymer-Bound Pyrene-4,5,9,10-tetraone for Fast-Charge and -Discharge Lithium-Ion Batteries with High Capacity. *J. Am. Chem. Soc.* **2012**, *134* (48), 19694−19700.

(8) Song, Z.; Qian, Y.; Liu, X.; Zhang, T.; Zhu, Y.; Yu, H.; Otani, M.; Zhou, H. A quinone-based oligomeric lithium salt for superior Li-organic batteries. *Energy Environ. Sci.* **2014**, *7* (12), 4077−4086.

(9) Song, Z.; Qian, Y.; Gordin, M. L.; Tang, D.; Xu, T.; Otani, M.; Zhan, H.; Zhou, H.; Wang, D. Polyanthraquinone as a Reliable Organic Electrode for Stable and Fast Lithium Storage. *Angew. Chem., Int. Ed.* **2015**, *54* (47), 13947−13951.

(10) Kwon, M.-S.; Choi, A.; Park, Y.; Cheon, J. Y.; Kang, H.; Jo, Y. N.; Kim, Y.-J.; Hong, S. Y.; Joo, S. H.; Yang, C.; et al. Synthesis of Ordered Mesoporous Phenanthrenequinone-Carbon via π-π Interaction-Dependent Vapor Pressure for Rechargeable Batteries. *Sci. Rep.* **2014**, *4* (1), 7404.

(11) Li, H.; Duan, W.; Zhao, Q.; Cheng, F.; Liang, J.; Chen, J. 2,2′-Bis(3-hydroxy-1,4-naphthoquinone)/CMK-3 nanocomposite as cathode material for lithium-ion batteries. *Inorganic Chemistry Frontiers* **2014**, *1* (2), 193−199.

(12) Zhang, K.; Guo, C.; Zhao, Q.; Niu, Z.; Chen, J. High-Performance Organic Lithium Batteries with an Ether-Based Electrolyte and 9,10-Anthraquinone (AQ)/CMK-3 Cathode. *Advanced Science* **2015**, *2* (5), 1500018.

(13) Zhao, L.; Lakraychi, A. E.; Chen, Z.; Liang, Y.; Yao, Y. Roadmap of Solid-State Lithium-Organic Batteries toward 500 Wh kg-1. *ACS Energy Letters* **2021**, *6* (9), 3287−3306.

(14) Su, Y.-S.; Manthiram, A. A new approach to improve cycle performance of rechargeable lithium-sulfur batteries by inserting a free-standing MWCNT interlayer. *Chem. Commun.* **2012**, *48* (70), 8817−8819.

(15) Hao, H.; Hutter, T.; Boyce, B. L.; Watt, J.; Liu, P.; Mitlin, D. Review of Multifunctional Separators: Stabilizing the Cathode and the Anode for Alkali (Li, Na, and K) Metal-Sulfur and Selenium Batteries. *Chem. Rev.* **2022**, *122* (9), 8053−8125.

(16) Song, Z.; Qian, Y.; Otani, M.; Zhou, H. Stable Li-Organic Batteries with Nafion-Based Sandwich-Type Separators. *Adv. Energy Mater.* **2016**, *6* (7), 1501780.

(17) Li, M.; Yang, J.; Shi, Y.; Chen, Z.; Bai, P.; Su, H.; Xiong, P.; Cheng, M.; Zhao, J.; Xu, Y. Soluble Organic Cathodes Enable Long Cycle Life, High Rate, and Wide-Temperature Lithium-Ion Batteries. *Adv. Mater.* **2022**, *34* (5), 2107226.

(18) Geng, K.; He, T.; Liu, R.; Dalapati, S.; Tan, K. T.; Li, Z.; Tao, S.; Gong, Y.; Jiang, Q.; Jiang, D. Covalent Organic Frameworks: Design, Synthesis, and Functions. *Chem. Rev.* **2020**, *120* (16), 8814−8933.

(19) Yuan, S.; Li, X.; Zhu, J.; Zhang, G.; Van Puyvelde, P.; Van der Bruggen, B. Covalent organic frameworks for membrane separation. *Chem. Soc. Rev.* **2019**, *48* (10), 2665−2681.

(20) Cao, Y.; Wu, H.; Li, G.; Liu, C.; Cao, L.; Zhang, Y.; Bao, W.; Wang, H.; Yao, Y.; Liu, S.; et al. Ion Selective Covalent Organic Framework Enabling Enhanced Electrochemical Performance of Lithium-Sulfur Batteries. *Nano Lett.* **2021**, *21* (7), 2997−3006.

(21) Xu, Q.; Zhang, K.; Qian, J.; Guo, Y.; Song, X.; Pan, H.; Wang, D.; Li, X. Boosting Lithium-Sulfur Battery Performance by Integrating a Redox-Active Covalent Organic Framework in the Separator. *ACS Applied Energy Materials* **2019**, *2* (8), 5793−5798.

(22) Wang, J.; Qin, W.; Zhu, X.; Teng, Y. Covalent organic frameworks (COF)/CNT nanocomposite for high performance and wide operating temperature lithium-sulfur batteries. *Energy* **2020**, *199*, 117372.

(23) Sun, K.; Wang, C.; Dong, Y.; Guo, P.; Cheng, P.; Fu, Y.; Liu, D.; He, D.; Das, S.; Negishi, Y. Ion-Selective Covalent Organic Framework Membranes as a Catalytic Polysulfide Trap to Arrest the Redox Shuttle Effect in Lithium-Sulfur Batteries. *ACS Appl. Mater. Interfaces* **2022**, *14* (3), 4079−4090.

(24) Burke, D. W.; Jiang, Z.; Livingston, A. G.; Dichtel, W. R. Two-Dimensional Covalent Organic Framework Membranes for Liquid-Phase Molecular Separations: State of the Field, Common Pitfalls, and Future Opportunities. *Adv. Mater.* **2023**, DOI: 10.1002/adma.202300525.

(25) Liang, Y.; Jing, Y.; Gheytani, S.; Lee, K.-Y.; Liu, P.; Facchetti, A.; Yao, Y. Universal quinone electrodes for long cycle life aqueous rechargeable batteries. *Nat. Mater.* **2017**, *16* (8), 841−848.

(26) Zhang, J.; Chen, Z.; Ai, Q.; Terlier, T.; Hao, F.; Liang, Y.; Guo, H.; Lou, J.; Yao, Y. Microstructure engineering of solid-state composite cathode via solvent-assisted processing. *Joule* **2021**, *5* (7), 1845−1859.

(27) Xing, C.; Chen, H.; Qian, S.; Wu, Z.; Nizami, A.; Li, X.; Zhang, S.; Lai, C. Regulating liquid and solid-state electrolytes for solid-phase conversion in Li-S batteries. *Chem.* **2022**, *8* (5), 1201−1230.
(28) Shevate, R.; Shaffer, D. L. Large-Area 2D Covalent Organic Framework Membranes with Tunable Single-Digit Nanopores for Predictable Mass Transport. *ACS Nano* **2022**, *16* (2), 2407−2418.
(29) He, A.; Jiang, Z.; Wu, Y.; Hussain, H.; Rawle, J.; Briggs, M. E.; Little, M. A.; Livingston, A. G.; Cooper, A. I. A smart and responsive crystalline porous organic cage membrane with switchable pore apertures for graded molecular sieving. *Nat. Mater.* **2022**, *21* (4), 463−470.
(30) Kandambeth, S.; Mallick, A.; Lukose, B.; Mane, M. V.; Heine, T.; Banerjee, R. Construction of Crystalline 2D Covalent Organic Frameworks with Remarkable Chemical (Acid/Base) Stability via a Combined Reversible and Irreversible Route. *J. Am. Chem. Soc.* **2012**, *134* (48), 19524−19527.
(31) Kandambeth, S.; Mallick, A.; Lukose, B.; Mane, M. V.; Heine, T.; Banerjee, R. Construction of Crystalline 2D Covalent Organic Frameworks with Remarkable Chemical (Acid/Base) Stability via a Combined Reversible and Irreversible Route. *J. Am. Chem. Soc.* **2012**, *134* (48), 19524−19527.
(32) Chang, Z.; Qiao, Y.; Deng, H.; Yang, H.; He, P.; Zhou, H. A Liquid Electrolyte with De-Solvated Lithium Ions for Lithium-Metal Battery. *Joule* **2020**, *4* (8), 1776−1789.
(33) Chang, Z.; Qiao, Y.; Yang, H.; Deng, H.; Zhu, X.; He, P.; Zhou, H. Beyond the concentrated electrolyte: further depleting solvent molecules within a Li+ solvation sheath to stabilize high-energy-density lithium metal batteries. *Energy Environ. Sci.* **2020**, *13* (11), 4122−4131.
(34) Xu, Q.; Tao, S.; Jiang, Q.; Jiang, D. Ion Conduction in Polyelectrolyte Covalent Organic Frameworks. *J. Am. Chem. Soc.* **2018**, *140* (24), 7429−7432.
(35) Singh, S.; Khulbe, K. C.; Matsuura, T.; Ramamurthy, P. Membrane characterization by solute transport and atomic force microscopy. *J. Membr. Sci.* **1998**, *142* (1), 111−127.
(36) Machado, D. o. R.; Hasson, D.; Semiat, R. Effect of solvent properties on permeate flow through nanofiltration membranes: Part II. Transport model. *J. Membr. Sci.* **2000**, *166* (1), 63−69.
(37) Deng, H.; Grunder, S.; Cordova, K. E.; Valente, C.; Furukawa, H.; Hmadeh, M.; Gándara, F.; Whalley, A. C.; Liu, Z.; Asahina, S.; et al. Large-Pore Apertures in a Series of Metal-Organic Frameworks. *Science* **2012**, *336* (6084), 1018−1023.
(38) Buchheim, J.; Schlichting, K.-P.; Wyss, R. M.; Park, H. G. Assessing the Thickness-Permeation Paradigm in Nanoporous Membranes. *ACS Nano* **2019**, *13* (1), 134−142.
(39) Lakraychi, A. E.; Dolhem, F.; Vlad, A.; Becuwe, M. Organic Negative Electrode Materials for Metal-Ion and Molecular-Ion Batteries: Progress and Challenges from a Molecular Engineering Perspective. *Adv. Energy Mater.* **2021**, *11* (32), 2101562.
(40) Nie, H. Y.; Walzak, M. J.; Berno, B.; McIntyre, N. S. Atomic force microscopy study of polypropylene surfaces treated by UV and ozone exposure: modification of morphology and adhesion force. *Appl. Surf. Sci.* **1999**, *144−145*, 627−632.
(41) Matsumoto, M.; Dasari, R. R.; Ji, W.; Feriante, C. H.; Parker, T. C.; Marder, S. R.; Dichtel, W. R. Rapid, Low Temperature Formation of Imine-Linked Covalent Organic Frameworks Catalyzed by Metal Triflates. *J. Am. Chem. Soc.* **2017**, *139* (14), 4999−5002.

https://doi.org/10.1021/acsenergylett.3c01740
ACS Energy Lett. 2023, 8, 5032−5040